Discrete dislocation modeling in three-dimensional confined volumes

Weygand, D.; Friedman, L.H.; van der Giessen, E.; Needleman, A.

Published in:
Materials science and engineering a-Structural materials properties microstructure and processing

DOI:
10.1016/S0921-5093(00)01632-4

Publication date:
2001

ELSEVIER

Materials Science and Engineering A309–310 (2001) 420–424

MATERIALS SCIENCE & ENGINEERING A

www.elsevier.com/locate/msea

Discrete dislocation modeling in three-dimensional confined volumes

D. Weygand [a], L.H. Friedman [a], E. van der Giessen [a], A. Needleman [b,*]

[a] *Micromechanics of Materials Group, Netherlands Institute for Metals Research, Delft University of Technology, Mekelweg 2, 2628 CD Delft, The Netherlands*

[b] *Division of Engineering, Brown University, Box D, Providence, RI 02912, USA*

Abstract

Plastic deformation of micron-sized specimens or smaller cannot be described by continuum plasticity, as the discrete nature of the dislocations can no longer be ignored. This paper presents a three-dimensional dislocation dynamics plasticity method developed for the study of plasticity of such small specimens. The approach includes two components: (i) plasticity is described by the dynamics of individual, discretized three-dimensional dislocation loops; (ii) a finite element model supplies 'image fields' that incorporate traction or displacement boundary conditions on the specimen.

A circular dislocation loop is used to validate the chosen discretization of the dislocation. The critical stress for activating a Frank–Read source confirms the used line-tension description. A tensile test of a free-standing thin film illustrates the incorporation of the boundary conditions into the model. Particular attention is given to the treatment of dislocation loops that have glided partly out of the body, leaving a step at the surface.

Keywords: Dislocation dynamics; Plasticity; Boundary effects; Thin films

1. Introduction

The development of small-scale structures and the study of their mechanical properties have revealed the limits of continuum plasticity to rationalize the observed properties [1]. Even though a continuum description of plastic flow has proved to be successful at macroscopic components (down to crystallites), provided that the appropriate constitutive laws are used, it implicitly assumes that the dislocation microstructure is important as an averaged quantity only. This no longer holds in micron-sized specimens, where the behaviour of individual dislocations or dislocation structures occurs on similar length scales as the size of the specimen. A model is needed where the (collective) behaviour of dislocations determines the plastic deformation response of a three-dimensional body subjected to specific boundary conditions. Since the length scale is substantially larger than the atomic scale, this is often referred to as the mesoscopic scale.

The modeling of the discrete dislocation behaviour at the mesoscopic level in two dimensions dates back to the late 1980s [2,3]. In the early 1990s, the interest in simulating curved dislocations in three dimensions [4,5] increased, as these simulations have the potential of making quantitative rather than just qualitative predictions.

Three-dimensional simulations give rise to new challenges. For example, they require adequate physical approximations for the treatment of junction formation/dissolution, cross-slip and climb [6] within the framework of mesoscopic dislocation models. Also, for micron-sized specimens, such as thin films, the boundary conditions are of paramount importance. The treatment of boundary effect has attracted little attention in these approaches. At the same time, it is equally important to understand how dislocations interact either with internal boundaries, such as in the presence of second-phase particles, particularly since size effects play a very large role at these size scales.

In 1995, Van der Giessen and Needleman [7] introduced a general method for the incorporation of boundary conditions in a discrete dislocation framework, valid for two and three dimensions. This method is able to handle arbitrary boundary conditions such as specified tractions or displacements, periodicity, or mixed conditions, using the finite element 'image' solution. Previous applications were in two dimensions only. Here we discuss details of the implementation for three dimensions.

2. Discrete dislocation framework

In a discrete dislocation plasticity description, dislocations are represented as line defects in a linear elastic continuum [6]. The evolution of the dislocation structure gives rise to what we observe as plastic deformation at a larger

* Corresponding author. Tel.: +1-401-863-2863; fax: +1-401-863-1157.
E-mail address: needle@engin.brown.edu (A. Needleman).

0921-5093/01/$ – see front matter
PII: S0921-5093(00)01632-4

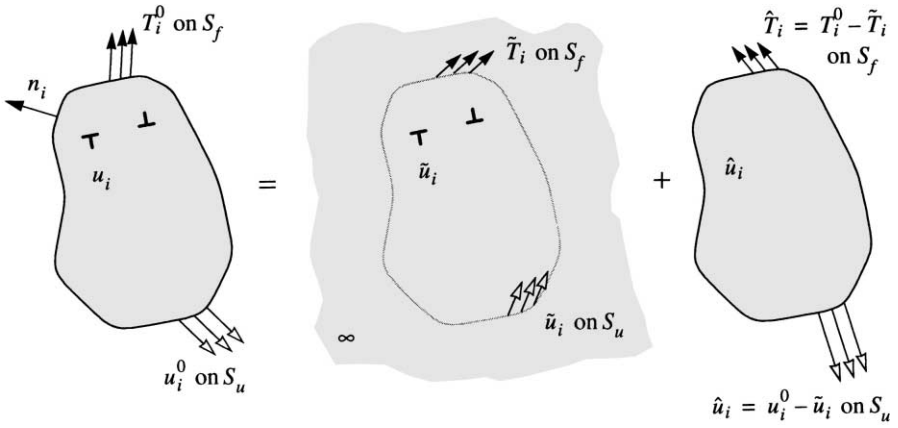

Fig. 1. Decomposition into the problem of interacting dislocations in the infinite solid (˜ fields) and the complementary problem for the finite body without dislocations (^ or image fields).

size-scale. In such a description, atomic-scale properties of dislocations or their interactions need to be supplemented through additional constitutive rules.

The simulation is carried out in an incremental manner. Each time step Δt involves three main computational stages: (i) determining the forces on the dislocations, i.e. the Peach–Koehler force; (ii) determining the rate of change of the dislocation structure, which involves the motion of dislocations, etc. and (iii) determining the stress and strain state for the updated dislocation arrangement, under the current boundary conditions. The first two will be discussed in more detail in the following section.

The determination of the state of stress, strain and displacement around any given dislocation requires the solution of a linear elastic boundary-value problem with discontinuities. Even for isotropic elasticity, such a solution is known in closed form only for very simple geometries, such as infinite space. The basic idea of the approach taken from [7] (see Fig. 1) is to split off the infinite-space solution that contains the dislocation singularity (to be identified by a (˜)) and to correct for the true boundary conditions through a correction field (to be identified by a (^)).

For homogeneous elastic materials, the latter 'image' (^)-fields satisfy the usual elasticity equations of compatibility, equilibrium and linear elastic constitutive law between stress and strain, subject to the boundary conditions

$$\hat{u}_i = u_i^0 - \tilde{u}_i \quad \text{or} \quad \hat{T}_i = T_i^0 - \tilde{\sigma}_{ij} n_j .$$

Here, u_i^0 and T_i^0 are the prescribed values of the displacements and tractions, respectively, on different parts of the boundary (with unit outer normal n_i) The (˜)-contributions to these expressions are the displacements and stresses at the boundary according to the infinite-space solution. The set of governing equations and boundary conditions contains no singularities and can be conveniently solved by a finite element method. The final solution for stress, strain and displacements is obtained as

$$\sigma_{ij} = \tilde{\sigma}_{ij} + \hat{\sigma}_{ij}, \qquad \epsilon_{ij} = \tilde{\epsilon}_{ij} + \hat{\epsilon}_{ij}, \qquad u_i = \tilde{u}_i + \hat{u}_i .$$

3. The 3D dislocation model

Dislocation loops are discretized by straight segments as illustrated in Fig. 2. As one goes around a dislocation loop, the type of the segments varies continuously from edge to screw. The nodes denoted by $\{\ldots, A-1, A, A+1, \ldots\}$ in Fig. 2 are the connection points of straight dislocation segments. These nodes are used to describe the dynamics of the dislocation structure.

The (˜)-stress field of each discretized dislocation is calculated using the analytical expressions given by Devincre [8]. The line tension contribution is incorporated using the Brown [9] scheme. The (˜)-displacement fields of the discretized dislocation loops are calculated as proposed by

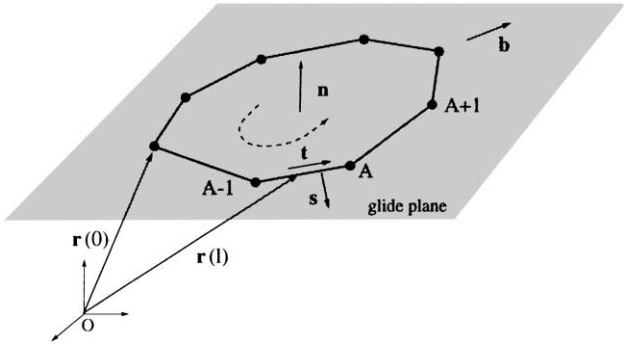

Fig. 2. Description of a dislocation loop in its glide plane; $\boldsymbol{n}$ is the normal vector of the glide plane; the orientation of the loop is given by the tangent vector $\boldsymbol{t}$ and the Burgers vector $\boldsymbol{b}$; $\boldsymbol{s}$ is defined as $\boldsymbol{t} \times \boldsymbol{n}$. A loop is confined to its glide plane. Cross-slipped dislocation loops are splitted into two loops that share one segment which is equivalent to a junction with zero net Burgers vector.

Barnett [10]. Strain fields are obtained by inverting the elastic constitutive law.

At present, the simulation aims to model conservative movement, i.e. dislocation glide. The glide velocity is taken proportional with the resolved Peach–Koehler force on the dislocation computed from both the $\tilde{\sigma}_{ij}$ of the dislocations and the image stress $\hat{\sigma}_{ij}$. Knowing the resolved Peach–Koehler force acting on the individual dislocation segments, the dynamics of segments is carried over to a dynamics of nodes connecting the segments using the integration scheme proposed by Kukta [11]. This scheme is in a sense equivalent to a one-dimensional finite element model for dislocation loops. The solution to the model is the set of nodal velocities for each dislocation.

The implementation of the dynamics contains several adaptation techniques. Knowing all nodal velocities, a maximal time step is calculated for each segment which is compatible with a chosen maximum relative length change for segments (≈20–50%). Furthermore, rotations of segments are controlled such that the maximum rotation during a time step is smaller than a threshold value on the order of ≈10–20°. The "best" values of relative angle and length change are being investigated. This procedure determines the time step Δt for the next increment. After having moved all dislocations during this time step, several options for the re-discretization of the dislocation structure are available. First, local adjustments are made on the basis of criteria involving the local curvature, the distance to the closest segment of a different loop (in plane/out of plane), and possible self-intersections of a loop. However, sometimes non-local adjustements are needed. For each segment, the individual maximum time step compatible with the mentioned conditions on relative length change and rotation is stored. The variation of these time steps along a loop is probed. When the variations are larger than one order of magnitude, the second procedure is performed. This procedure entails a redistribution of the nodal points of that loop using a curvature-weighted spline. These two procedures are never applied during the same time step; the frequency of application is a parameter to be explored further.

As mentioned in Section 2, the ($\hat{}$)-fields, determined by a finite element method, allow one to handle dislocations in confined volumes and to incorporate the boundary conditions. A feature of three-dimensional dilocation plasticity that requires special attention in this respect is that dislocations that are initially inside the body may glide out of it, thus leaving a step at the surface. This is handled as follows: the dislocation is splitted in an "in-volume part" and an "out-of-volume" part. These parts are joined at nodes which can only move along the surface of the body. For this purpose, the surface of the volume is described by triangles, which allow to approximate complex boundary shapes. The surface step thus arises naturally from the discontinuity in the ($\tilde{}$)-displacement field. The out-of-volume part is evidently artificial, but its effects will be corrected through the ($\hat{}$)-fields. In fact, the location of the outside dislocation segments is arbitrary, and the ($\hat{}$)-fields will take care of the correct boundary conditions. This is true for very fine finite element meshes. For coarser meshes, the accuracy of the final solution can be improved by a proper choice for the location of the outside segments to mimic local mirror-images of dislocations.

4. Validation tests

The accuracy of the chosen description has been validated with respect to two aspects: (i) geometrical discretization errors due to the straight-line approximation between nodes and (ii) the calculation of the line tension. Both are coupled since the curvature of the dislocation is controlled by the chosen discretization. In the straight-line approximation, the curvature localizes at nodal points. Therefore, the variation of the stress fields of neighbouring segments around the common node is rather important, and varies roughly as $(1/(r + a))$, where r is the distance from that common nodal point and a is of the order of the 'cut-off' distance/displacement in the Brown procedure. Therefore, for next-neighbour interactions, Gauss integration with a large number (up to 50) of integration points is used to capture this variation.

Fig. 3 shows the relative error in the nodal force for the nodes of a circular dislocation loop, for different radii and for different discretizations and number of integration points per segment. The numerical results are compared with an analytical solution for the resolved Peach–Koehler force for a circular loop according to [11]. Note that the relative error in the nodal force decreases monotonically with increasing number of integration points and segments.

One observes that the error for the larger loops decreases less rapidly with increasing number of integration points.

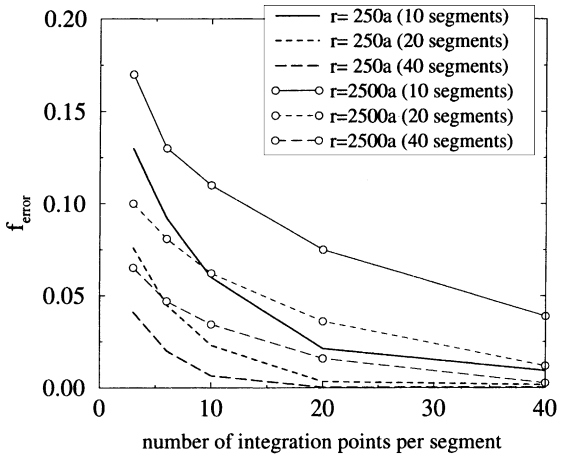

Fig. 3. Relative error, $f_{\text{error}} = (1/n)\sqrt{\sum_{i=1}^{n}((f_{\text{analytical}} - f_{\text{model}})/f_{\text{analytical}})^2}$ of the nodal force for circular dislocation loops of different sizes using different discretizations.

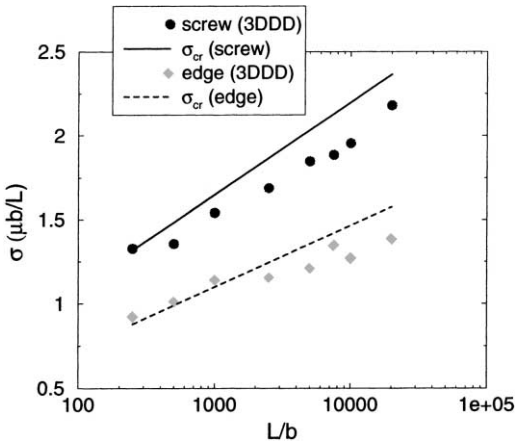

Fig. 4. Critical activation stress of edge and screw Frank–Read sources of arm length L.

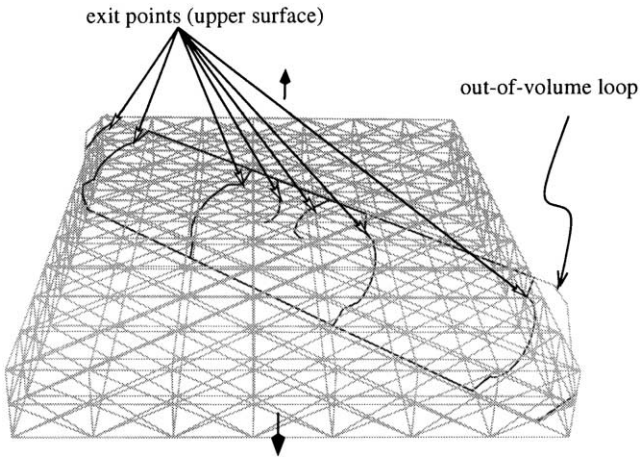

Fig. 5. Free-standing thin film under tension. The central Frank–Read source has emitted several dislocation loops which have left the film either partly or completely. A coarse finite element mesh is used just to increase the visibility of the dislocations.

This can be understood by noting that the length of the segments increases with the loop radius, but that the locations of the Gauss integration points are relative to the segment length. In order to capture the strong $(1/(r+a))$-dependency in the stress field of the neighbouring segments, more integration points are therefore needed. However, it is not necessary to evaluate the nearest neighbour stress fields explicitly at all integration points. The approximate functional form $(1/(r+a))$ is fitted to the nearest neighbour contribution to the resolved shear stress evaluated at a few points only. Then, this fit is integrated using a large number of Gauss-quadrature points.

The second test is concerned with the critical activation stress of an open-armed Frank–Read source. Numerical results are compared in Fig. 4 to the expression [12],

$$\sigma = \frac{A}{(2\pi)}\mu\left(\frac{b}{L}\right)\log\left(\frac{L}{r_0}\right)$$

where μ is the shear modulus, ν the Poisson's ratio, L the arm spacing and r_0 the cut-off length. The value of A is 1(or $1/(1-\nu)$) for initially edge (or screw) oriented sources. The logarithmic line tension contribution to the critical stress is reproduced.

The formation and destruction of junction is included in the model. The criterion for formation is the reduction of the elastic energy. A junction is taken to dissolve as soon as its length shrinks to a threshold value which is on the order of some Burgers vectors.

5. Example and conclusion

The emphasis of this approach lies in the capability to solve three-dimensional boundary value problems for dislocated bodies, in the field of three-dimensional discrete dislocation plasticity modeling, incorporating the singular stresses and discontinuous displacements caused by the dislocations. The most important aspects are illustrated by a free-standing thin film under tension as shown in Fig. 5. This example involves mixed boundary conditions: normal displacements are prescribed to two opposite faces of the film leads to in-plane tension in the film, while the shear tractions on these faces are assumed to vanish. The remaining faces are assumed to be completely traction free.

A Frank–Read source has been placed in the centre of the film as shown in Fig. 5. As the end displacements are prescribed to grow in time at a constant rate, a stress state builds up in the film that is uniform except near the Frank–Read source. Under the influence of this stress, the Frank–Read source bows out and generates a new loop. As this loop further expands, parts of it are attracted by the traction-free upper and lower surfaces and leave the film there, leaving a step. Fig. 5 shows a situation at which several loops have already nucleated. The out-of-volume dislocation segments that 'virtually' close the dislocation outside the film are shown explicitly to emphasize the procedure described in Section 3. One loop has already left the volume entirely. Its exit points at the free upper and lower surfaces have moved around the side face and joined each other. A step that is exactly equal to the length of the Burgers vector is going around the surface of the film.

This example shows that the method presented here is capable of modeling the whole sequence from generation of the loop by means of an activated Frank–Read source to the formation of a complete slip step, created by a dislocation leaving the volume.

References

[1] Y.-L. Shen, S. Suresh, M.Y. He, A. Bagchi, O. Kienzle, M. Rühle, A.G. Evans, J. Mater. Res. 13 (1998) 1927–1937.
[2] J. Lépinoux, L.P. Kubin, Sci. Metall. 21 (1987) 833.
[3] R.J. Amodeo, N.M. Ghoniem, Phys. Rev. B 41 (1990) 6958.

[4] L.P. Kubin, G. Canova, M. Condat, E. Devincre, V. Pontikis, Y. Bréchet, in: G. Martin, L.P. Kubin (Eds.), Nonlinear Phenomena in Materials Science II, Sci-Tech, Vaduz., 1992, p. 455.
[5] H.M. Zbib, M. Rhee, J.P. Hirth, Int. J. Mech. Sci. 40 (1998) 113–127.
[6] J.P. Hirth, J. Lothe, Theory of Dislocations, 2nd Edition, Wiley, New York, 1982.
[7] E. Van der Giessen, A. Needleman, Model. Simul. Mater. Sci. Eng. 3 (1995) 689.
[8] B. Devincre, Solid State Commun. 93 (1995) 875.
[9] L.M. Brown, Philos. Mag. 10 (1964) 441.
[10] D.M. Barnett, Philos. Mag. A 51 (1985) 383.
[11] R.V. Kukta, Ph.D. thesis, Brown University, May 1998.
[12] A.J.E. Foreman, Philos. Mag. 15 (1967) 1011.